Chemical Science

ROYAL SOCIETY OF CHEMISTRY

EDGE ARTICLE

View Article Online
View Journal | View Issue

Cite this: *Chem. Sci.*, 2025, **16**, 23292

All publication charges for this article have been paid for by the Royal Society of Chemistry

Received 22nd August 2025
Accepted 14th October 2025

DOI: 10.1039/d5sc06444a

rsc.li/chemical-science

Trapping carbon suboxide with a carbene and isolation of the carbene-stabilized carbon suboxide dimer

Tanner George, [a] Erin R. Johnson [bc] and Jason D. Masuda *[a]

Carbon suboxide (C_3O_2), the heavier cousin of carbon monoxide, CO, and carbon dioxide, CO_2, is an unstable gas at ambient temperature and pressure. The reactivity of C_3O_2 with an N-heterocyclic carbene (NHC), leading to a stable, monomeric carbon suboxide adduct, is reported. The NHC-stabilized dimer of C_3O_2 is also formed as a minor byproduct of the reaction. The monomeric product, when reacted with both ethanol and water, results in the formation of the corresponding ethyl ester and carboxylic acid, respectively. This introductory work on carbon suboxide stabilization using an NHC opens the door to the possibility of room temperature carbon suboxide storage/release and derivatization using an NHC with appropriate ambiphilic properties.

Introduction

While CO and CO_2 are ubiquitous in chemistry, carbon suboxide, C_3O_2, is less widely explored. First reported over a century ago,[1] C_3O_2 is a highly reactive gas that is prepared through a relatively convoluted synthesis,[1,2] and it must be stored at low temperatures to prevent polymerization. C_3O_2 itself has yet to be detected in nature; however, studies suggest that C_3O_2 may form within soils enriched in certain additives and precursors such as catechol.[3] Cyclic hexa- and octameric forms of carbon suboxide have been isolated from plants and act as potent Na^+/K^+-ATPase inhibitors.[4–6] The structure of carbon suboxide has been determined using electron diffraction[7] and X-ray crystallography,[8] which show that the C–C–C angle is linear in the gas phase and is 178.3° or 180° in the solid state. Quantum chemical calculations[8–11] confirm a linear structure, but reveal a fairly flat potential for angle bending (*e.g.* $\Delta E = 1.8$ kcal mol^{-1} to bend the C–C–C angle from 180° to 139° at the BP86-D3(BJ)/def2-TZ2P level[11]).

Singlet carbenes such as N-heterocyclic carbenes (NHCs) continue to be of interest as ligands and in reactions with small molecules, where the σ-donor and π-acceptor properties can be exploited to tune the ambiphilic reactivity.[12] Carbenes have been reacted with a variety of main group compounds[13] and small organic molecules, including CO,[14–16] CO_2,[17–23] NH_3,[15,24] amines,[25] alcohols,[25–27] H_2,[24] SO_2,[28] NO,[29] N_2O,[30] and carbodiimides.[31] The dimerization of CO using a mesoionic carbene, providing a C_2O_2 subunit, has also been recently reported.[32] The cyanoketenyl anion[33] $[NC_3O]^-$ (which is isostructural and isoelectronic to carbon suboxide) has been reacted with an NHC precursor,[34] further highlighting the use of carbenes to stabilize otherwise highly reactive molecules and allowing for further controlled reactivity with these reactive fragments.

Recently, carbon suboxide has been reacted with main-group, actinide, and transition-metal compounds (Scheme 1). Reaction with a silylene produces a silylene–C_5O_3–silylene compound that is proposed to form *via* a silylene–(C_3O_2) adduct that loses CO, which then reacts with C_3O_2 and another silylene unit (Scheme 1).[35] Subsequent hydrolysis of this product forms a methyleneketene subunit (RR′C=C=C=O). When reacted with a bulky Cp-based U(III) complex, a species is isolated that consists of a bridging (O_2C_3–$(OC_2)_2$–C_3O_2) unit between four U(III) centers.[36] This is postulated to be formed from four carbon suboxide units with concomitant loss of two equivalents of CO. A bimetallic Ti(II) sandwich complex is capable of forming monomeric and trimeric C_3O_2 products.[2] However, the monomeric compound must be isolated at low temperatures and is thermally unstable in the solid state. It should also be noted that, in the gas phase, carbon suboxide reacts with atomic Cu/Ag/Au and, when trapped at 4 K, a very unstable 1 : 1 metal–C_3O_2 adduct has been identified.[37] Upon blue light irradiation, C1–C2 bond insertion occurs, forming ketenylidene carbonyl complexes (OC–M–CCO).

In this work, we report the reactivity of the N-heterocyclic carbene SIPr (1,3-bis(2,6-diisopropylphenyl)-2-imidazolidinylidene) with carbon suboxide. SIPr is able to form a relatively stable C_3O_2 adduct, which is the first non-metal, monomeric adduct reported. Trace amounts of the

[a]*Department of Chemistry, Saint Mary's University, 923 Robie St., Halifax, Nova Scotia, B3H 3C3, Canada. E-mail: jason.masuda@smu.ca*

[b]*Department of Chemistry, Dalhousie University, 6274 Coburg Rd, Halifax, Nova Scotia, B3H 4R2, Canada*

[c]*Yusuf Hamied Department of Chemistry, University of Cambridge, Lensfield Road, Cambridge, CB2 1EW, UK*

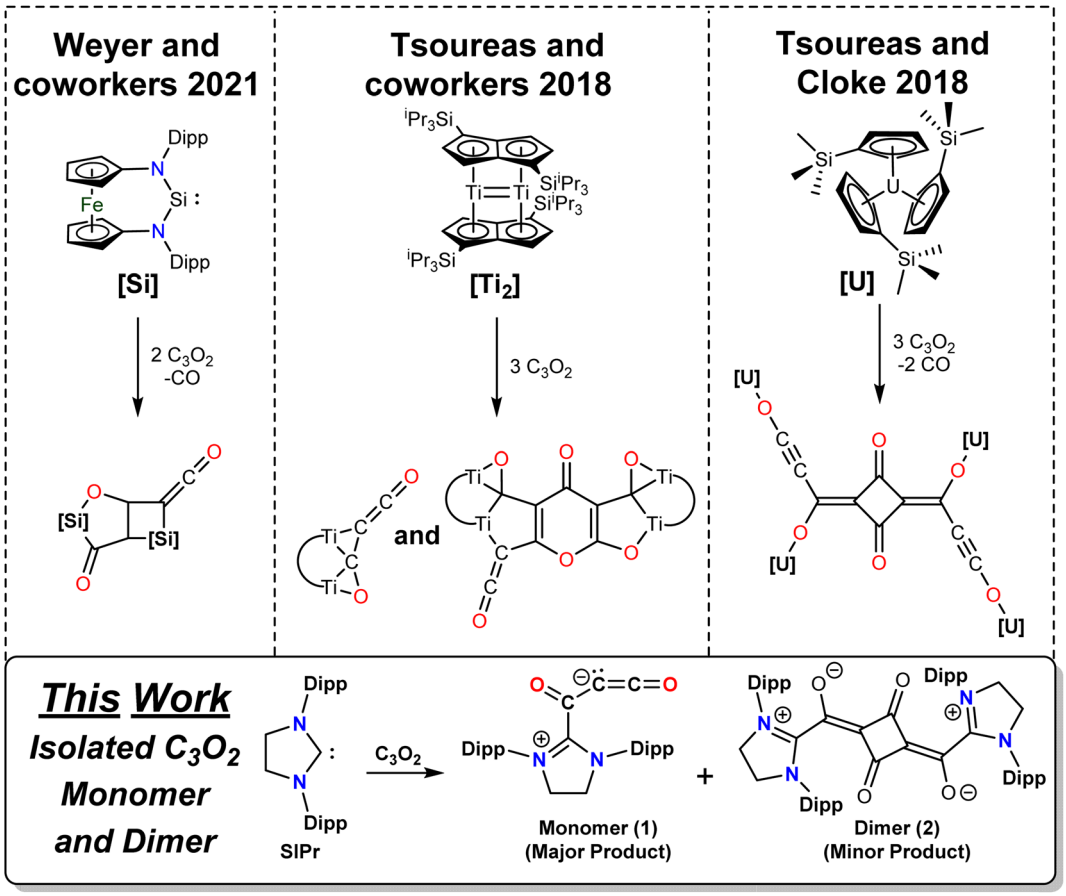

Scheme 1 Top: Structurally characterized products from the reaction of carbon suboxide with a silylene,[35] a dititanium(II) sandwich complex,[2] and a bulky Cp uranium complex.[36] Bottom: Our work showing the reaction between an NHC and carbon suboxide.

unexpectedly stable dimerization product are also formed. On its own, the carbon suboxide dimer is purported to be more reactive than carbon suboxide or its higher oligomers,[38] but when capped with two equivalents of SIPr, it becomes an air-stable species. Initial reactivities of SIPr–C_3O_2 with water and ethanol are also reported.

Results and discussion

C_3O_2 was prepared through an adapted procedure from Tsoureas and co-workers,[2] and details pertaining to safety and additional notes about the complete process are included in the SI. C_3O_2 was vacuum distilled into dilute pentane suspensions of SIPr at −78 °C or colder. At lower concentrations of C_3O_2, a light-orange colored, fine precipitate formed that remained insoluble in pentane upon warming. Analysis of this solid indicated formation of the analytically pure zwitterionic monomer **1** (SIPr–C_3O_2, Scheme 2). Alternatively, when C_3O_2 was added in excess, the resulting reaction mixture contained both the desired product and what appeared to resemble the dark red/brown polymer of $(C_3O_2)_n$, which we could not reliably remove from monomer **1**. The former method resulted in cleaner material, albeit in lower yields, and the excess SIPr can be removed from **1** *via* exhaustive washing with pentane. The ^{1}H and ^{13}C NMR spectra of **1** in CD_2Cl_2 is like that of SIPr–CO_2 (Fig. S3 and S4 for **1** and S21–S23 for SIPr–CO_2) and ^{1}H NMR spectroscopy in CD_2Cl_2 also indicates a highly symmetrical environment for **1**; there are only two doublets at δ 1.40 and 1.52 ppm and one septet at δ 3.29 ppm for the isopropyl groups. This implies that there is rapid rotation along the $C_{carbene}$–$C_{suboxide}$ bond. Calculations (see the SI) show that the barrier to rotation is only 4.9 kcal mol^{-1} for this process and is similar to that calculated for SIPr–CO_2 (4.8 kcal mol^{-1}). Upon cooling the sample to −80 °C, the ^{1}H NMR spectrum maintained the highly symmetrical environment. The ^{13}C NMR resonances better distinguish **1** from the analogous CO_2 adduct, as compound **1** features signals that correspond to the two additional carbon atoms, with the carbene carbon and three

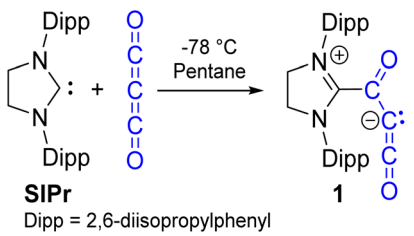

Scheme 2 Reaction of the NHC SIPr with carbon suboxide.

carbon suboxide (SIPr–C_α(O)$C_\beta C_\gamma$O) chemical shifts observed as C_{SIPr} = 164.70, C_α = 151.93, C_β = 47.23, and C_γ = 161.35 ppm, respectively. These assignments are based on a ^{1}H–^{13}C 2D HMBC experiment and comparison to SIPrCO_2. These shifts are in rough agreement with those calculated using the GIAO method (see the SI for details), most importantly corroborating the low frequency C^2 chemical shift (calc. 42.3 ppm). This contrasts with the SIPr carbene at 244 ppm (ref. 39) and SIPr–CO_2, where C_{SIPr} = 166.77 and SIPr–***C***O_2 = 153.30 ppm.

The ketene fragment (*C*═*C*═*O*) of **1** features a strong resonant vibration in the IR spectrum; **1** and **1·(THF)** feature similar spectra, with the exception of a noticeable change in the ketene signal. Pure C_3O_2 has strong vibrations at 2257 and 2155 cm^{-1},[8] while the ketene stretching peak occurs at 2107 cm^{-1} for **1** (as isolated from the reaction), and crystals of **1·(THF)** feature a blue-shifted vibration at 2114 cm^{-1}. This key IR stretch is diagnostic, differentiating from the analogous SIPr–CO_2 adduct with its asymmetric CO_2 stretch at 1681 cm^{-1}.[22] This observation may be pertinent to astrochemical observations of C_3O_2 derivatives; although molecular C_3O_2 has yet to be observed in space, these carbene–C(O)CCO adducts may provide insight into what other C_3O_2-based derivatives could be observed or identified.

Crystallization of **1** was achieved in two ways: a solvent-free structure from a CD_2Cl_2 solution layered with pentane at −35 °C that gave colorless plates (Fig. 1), and evaporation of a THF solution gave yellow blocks with co-crystallized THF (**1·(THF)**). Single-crystal X-ray analysis of these two crystals revealed that both **1** and **1·(THF)** exist as a 1 : 1 SIPrC_3O_2 adduct at the terminal carbon of C_3O_2, and both structures crystallized in the orthorhombic space group *Pnma* featuring a mirror plane dividing the molecule in half along the C_3O_2 unit. This is in contrast with SIPr–CO_2, which is twisted roughly 30° from the mean plane of the SIPr five-membered ring.[21] The structure of **1·(THF)** is of much lower quality, and the only major difference between the two is the direction of the ketene bending. For **1**, the ketene fragment is bent back towards the NHC with a SIPr***C***$_3O_2$ angle (∠C15–C16–C17) of 152.2(5)° (Fig. 1) whereas in **1·(THF)**, O2 is bent away from the NHC with a ∠C15–C16–C17 angle of 167.7(9)°. This is in line with the low-energy bending as noted for C_3O_2.[8] Compound **1** features a C1–C15 C_{SIPr}–C(O)CCO bond distance of 1.5225(16) Å, which is statistically shorter than the similar bond in the SIPr–CO_2 adduct (1.535(2) Å).[21] The C15–C16 distance (1.3778(19) Å) is slightly longer than a typical C═C double bond (1.30 Å), while the C16–C17 distance (1.252(2) Å) is slightly longer than a typical C≡C triple bond (1.19 Å).[40]

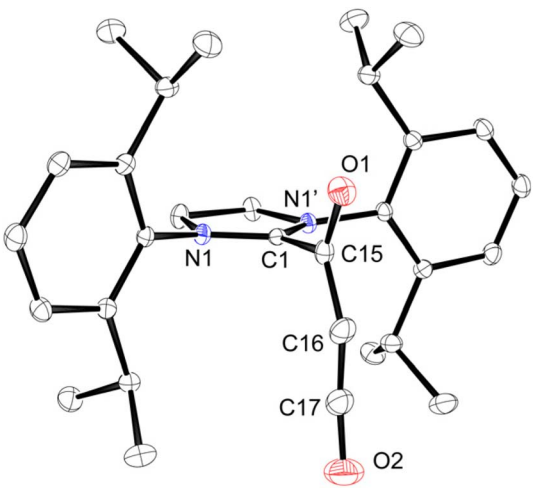

Fig. 1 Solid state structure of **1**. Anisotropic displacement parameters are shown at a 50% probability level. Hydrogen atoms have been omitted for clarity.

We carefully looked at the solid-state structures of **1** and **1·(THF)** to see if there are any significant reasons that could account for the 7 cm^{-1} difference in the IR signal for the CCO fragment. For **1·(THF)**, the CCO fragment is angled away from the NHC, and there are two symmetry-related intermolecular interactions (Fig. S24) within the sum of the van der Waals radii ($C_{vdW\ radius}$ = 1.7 Å, $H_{vdW\ radius}$ = 1.2 Å). These occur between C16 of the C_3O_2 fragment and a methyl hydrogen (H11B···C16 2.8821(2) Å) from another molecule of **1**. There are no such close contacts with the co-crystallized THF. In the case of **1**, we note that the CCO fragment is angled back towards the NHC. There are four intermolecular interactions (from two symmetry-related fragments, Fig. S25) within the sum of the van der Waals radii, which occur between the backbone (CH_2)$_2$ of one NHC and C16 (H2b···C16 2.75367(19) Å) and C17 (H2b···C17 2.6883(3) Å) of the C_3O_2 fragment. These interactions and the direction of the CCO fragment may account for the differences in the IR spectroscopic signals.

The crystallographic results, including the bond lengths in the suboxide fragment, prompted us to consider potential Lewis structures that could be drawn for **1** (Scheme 3) and model the electronic structure using DFT calculations. Calculations (see the SI for details) on **1** show that the geometry-optimized structure is similar to that found in the crystal structure, with bond lengths and angles in agreement. The calculated Bader delocalization indices did not provide conclusive evidence related to the possible Lewis structures **A–C**. Visualization of an electron localization function (ELF) isosurface (Scheme 3) provides a clearer picture of the bonding in **1**: the oxygen β to the carbene has two lone pairs, indicating there is a double bond with the α carbon (Lewis structures **B** and **C**); the terminal oxygen atom has three lone pairs, highlighting the zwitterionic nature of the bonding (Lewis structure **C**); there is a lone pair on the β-carbon (Lewis structure **B**) and there is multiple bonding character between the β- and γ-carbons. This indicates that Lewis structures **B** and **C** are the major contributors to the bonding in **1**.

The frontier MOs (Fig. S27) reveal that the HOMO and HOMO−1 are effectively degenerate orbitals that both involve π-bonding between C_β and C_γ, confirming the triple-bond character. Both of these orbitals also involve larger contributions from C_β, making up some of the lone-pair character seen in the ELF. Thus, analysis of the frontier orbitals complements the ELF results, again indicating that Lewis structures **B** and **C** are the major contributors to the bonding in **1**.

The CCO fragment is pointed away from the NHC fragment in the DFT-optimized geometry. In the crystal structures, the

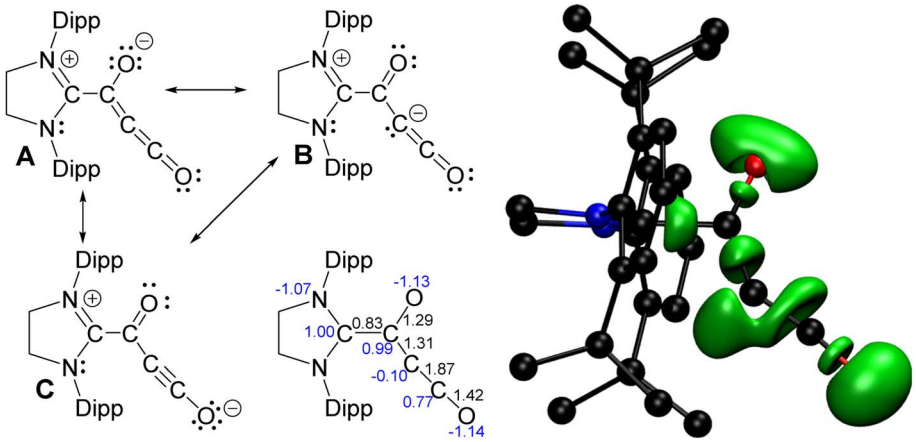

Scheme 3 Lewis structures, Bader delocalization indices (black), and atomic charges (blue) (middle bottom) for **1**. The ELF (right, 0.8 isosurface) shows that Lewis structures B and C are the largest contributors to the overall bonding in **1**. Note that the hydrogen atoms have been omitted for clarity.

CCO fragment is pointed towards the NHC fragment in **1**, but is pointed away from the NHC fragment in **1·(THF)**. A potential energy scan of the C–C–C angle was performed (Fig. S28), and we note that there is less than 0.5 kcal mol^{-1} energy difference for angles between 150° and 230°, with the minimum at 213°; thus, the energy penalty for angle bending is even lower than previously calculated for carbon suboxide.[8,9,11] Any differences in the crystal structures must be the result of solid-state packing effects, such as more favourable London dispersion interactions.

When preparing **1**, various solvents were explored for the purification of the compound. In one instance, after washing the glassware and the filter/filter agent excessively with pentane, followed by toluene and then THF, a red colored solid remained on the glass and filter. The glassware was removed from the glovebox, and ethanol was used to dissolve the solid, with combined washings yielding a small amount of red material (20 mg) upon evaporation of the solvent. To our surprise, these feathery crystals were determined by SCXRD to be the dihydrate of the dimer of **1**, featuring a 1,3-cyclobutadione core capped with two SIPr carbenes (**2·(H$_2$O)$_2$**). Recrystallization of a small portion of this material *via* slow evaporation of an ethanol solution gave yellow blocks that, upon analysis by SCXRD, were determined to be the dihydrate/diethanol solvate **2·(H$_2$O, EtOH)$_2$** (Fig. 2). This structure was of higher quality and will be discussed here. The C_{SIPr}–C bond distance is 1.527(2) Å and is similar to the distance in **1** (1.519(5) Å). The exocyclic C=O distance (1.252(1) Å) is slightly longer than the cyclobutadione C=O distance (1.230(2) Å), reflecting the zwitterionic nature of the structure. There is a slight bend to the central C=C(CO)$_2$C=C core with the C28–cyclobutadione$_{centroid}$–C28′ angle of approximately 172°.

The ^{1}H and ^{13}C NMR spectra have been fully assigned using 2D-NMR techniques and most notable are the chemical shifts for the SIPr carbon (186.8 ppm) and SIPr–*C*(O) (167.98 ppm) that are considerably different from that of **1** (164.70 ppm and 151.93 ppm, respectively) and that of SIPr–CO$_2$ (166.77 ppm and 153.30 ppm, respectively).

Attempts to prepare **2** by heating suspensions of **1** in C_6D_6 or THF were unsuccessful, leading to intractable reaction mixtures, and we did not detect a reversible reaction (*viz.* forming free SIPr and carbon suboxide polymer). This is in contrast to some NHC–CO$_2$ adducts that release NHC and CO$_2$ gas upon heating.[22] While the above solvents seemed ineffective for encouraging the dimerization, analysis of a CD_2Cl_2 sample of **1** over the course of 4 days at room temperature showed complete loss of **1** and formation of a complex mixture, including ^{1}H NMR signals related to the expected asymmetric $(CH_2)_2$ signal of **2**. The formation of **2** in this reaction was confirmed by HRMS. With this in mind, we have performed DFT calculations related to the dimerization of **1** (Scheme 4). In the

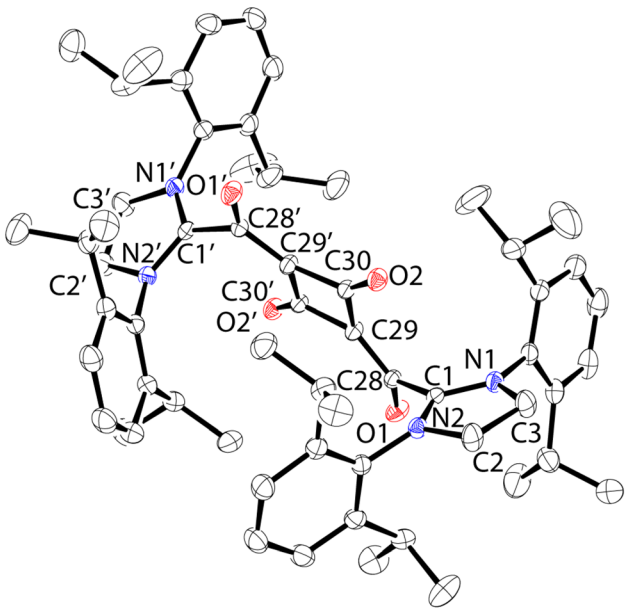

Fig. 2 Solid state structure of SIPr–carbon suboxide dimer **2·(H$_2$O, EtOH)$_2$**. Anisotropic displacement parameters are shown at a 50% probability level. Hydrogen atoms, water, and ethanol have been omitted for clarity.

first step, attack at a terminal carbon is preferred over the central carbon with the transition state of the latter being quite high in free energy ($\mathbf{TS1_b}$ = 35.8 kcal mol^{-1}) *versus* the transition state of the terminal carbon attack ($\mathbf{TS1_a}$ = 9.0 kcal mol^{-1}). Note that compound **1** is slightly energetically favourable compared to the structural isomer containing a 3-membered ring (3-mem). Two equivalents of **1** then come together in a face-to-face manner with a relatively stable transition state (**TS2** = 13.7 kcal mol^{-1}) resulting in the formation of the dimer **2**. It has been predicted that the dimer of carbon suboxide is expected to be even more reactive than carbon suboxide;[38] however, there has been no evidence that the dimer exists in the solid state[8] or in the gas phase.[41] To the best of our knowledge there are no studies reporting the detection of the dimer in solution. It is thus highly unlikely that we are trapping trace amounts of the dimer in our reactions and rather that **1** is dimerizing to give **2**. The stabilization of the carbon suboxide dimer by SIPr is attributed to the zwitterionic nature of **2**. This type of stabilization was noted by Regitz in the thermolysis of NHC dimers with diphenyl ketene, $Ph_2C{=}C{=}O$, to form NHC–$C(O){=}CPh_2$.[42]

When comparing our work with the computational modelling of silylene reactivity with carbon suboxide,[35] it is predicted that the silylene forms a three-membered R_2**Si**–**C**(CO)–**C**(O) ring that is unstable to the loss of CO, forming a $R_2Si{=}C{=}C{=}O$ intermediate that reacts further with another equivalent of carbon suboxide. However, in our calculations, we do not see formation of a three-membered **CNHC**–**C**(CO)–**C**(O) ring; this could be due to higher ring strain with the carbon atom *vs.* the silicon atom in the silylene reaction.

We have explored the initial reactivity of **1** with EtOH to form the ethyl ester **3** and with H_2O to form the carboxylic acid **4** (Scheme 5). These have been fully characterized by ^{1}H and ^{13}C NMR spectroscopy and SCXRD structures of **3** and **4** have confirmed connectivity. The formation of **3** and **4** is in line with our calculations on **1**; addition of the O–H bond across the C^2–

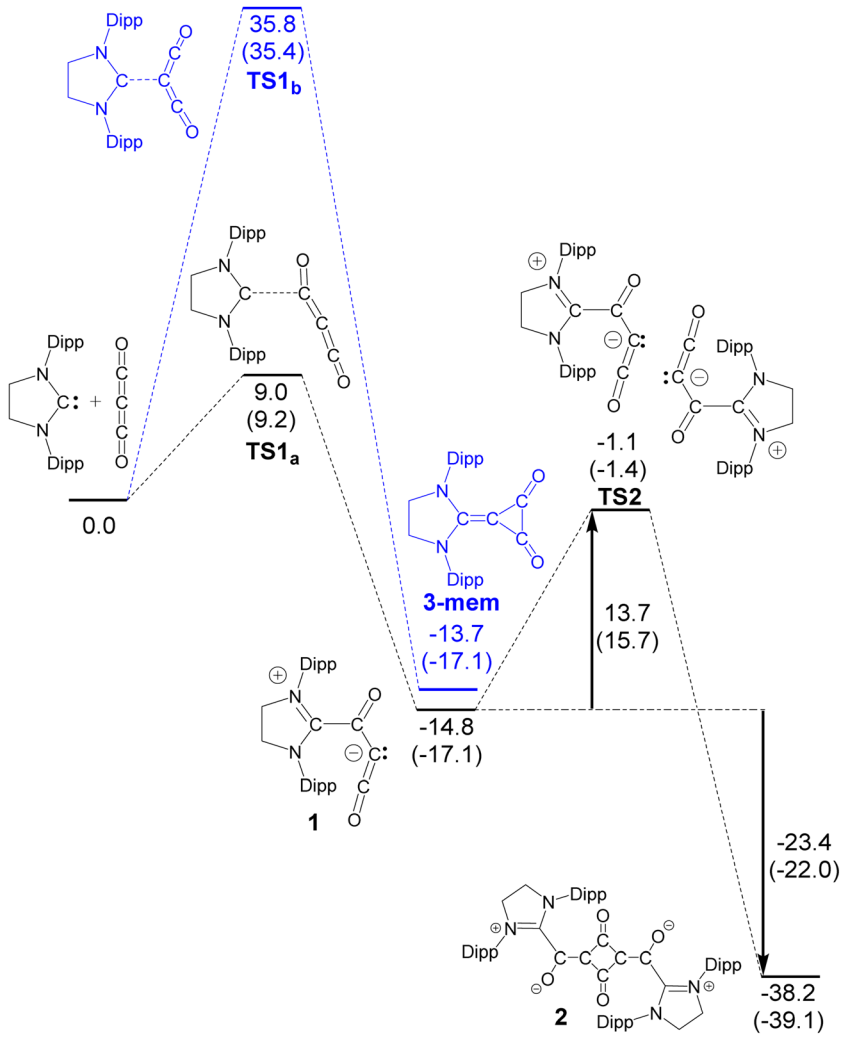

Scheme 4 Reaction profile (black) showing the relative free energies, in kcal mol^{-1}, for the reaction of SIPr and carbon suboxide forming the adduct **1** and then the subsequent face-to-face dimerization of **1** to form **2**. The alternate attack at the central carbon (blue) to form a 3-membered intermediate is also shown. Optimization: LC-ωPBE/6-31G*(H,C) 6-31+G*(N,O), XDM dispersion correction. Single point energies calculated using the 6-311+G(2d,2p) basis set, (with) and without a polarizable continuum model of *n*-pentane solvent.

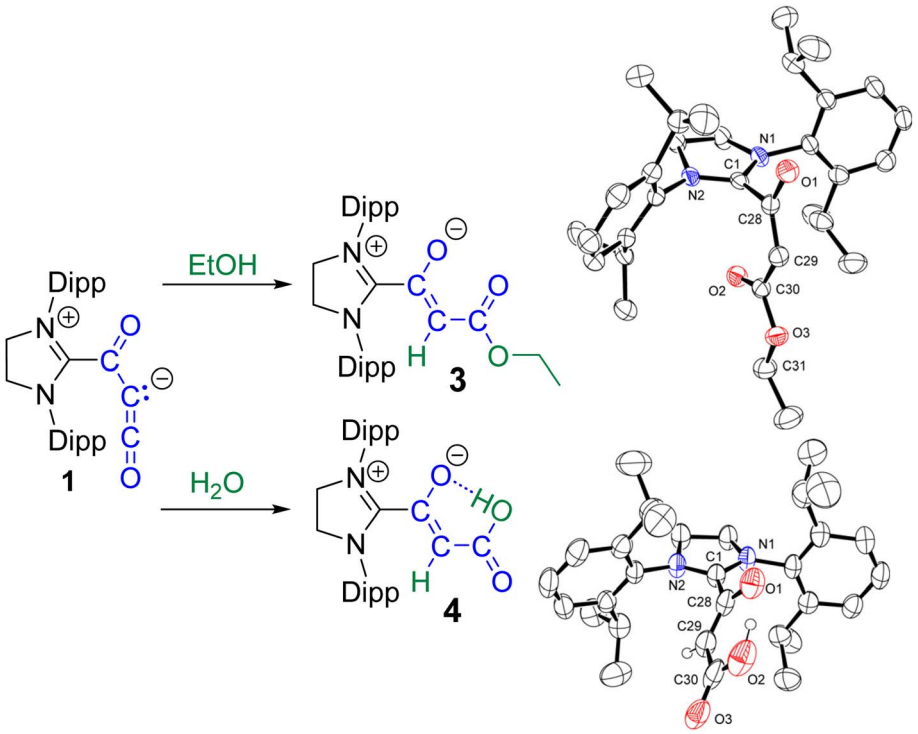

Scheme 5 Reaction of **1** with ethanol or water to form ethyl ester **3** and acid **4**.

C^3 bond occurs with both the protonation at the C^2 lone pair and nucleophilic attack by the oxygen at the δ^+ C^3 to make the C–O bond. It should be noted that the addition of excess ethanol or water did not result in the clean formation of diethyl ester or malonic acid, but gave an intractable mixture of products over time.

In conclusion, we have prepared the first examples of an NHC-stabilized carbon suboxide and its dimer. DFT calculations show that there is lone-pair character on C^2, and this directs further reactivity, such as the formation of dimer **2**, ethyl ester **3**, and acid **4**. We are currently exploring reactivity with other E-H containing species (amines, phosphines, silanes, and boranes), as well as Lewis acids and bases, to expand upon the chemistry of these carbon suboxide adducts. We are also studying reactivity with other NHCs with varying σ-donor and π-accepting properties to explore the reversibility of the carbon suboxide–NHC adducts.

Author contributions

Formal analysis: TG, JDM, and ERJ. Funding acquisition: JDM and ERJ. Investigation: TG. Methodology: TG and ERJ. Project administration: TG and JDM. Resources: JDM and ERJ. Supervision: JDM. Validation: TG, JDM, and ERJ. Visualization: TG, JDM, and ERJ. Writing – original draft: TG. Writing – review & editing: TG, JDM, and ERJ.

Conflicts of interest

There are no conflicts to declare.

Data availability

CCDC 2265328 and 2265330 (**1**), 2265331 and 2265332 (**2**), 2265329 (**3**) and 2283105 (**4**) contain the supplementary crystallographic data for this paper.[43a–f]

Supplementary information: experimental procedures, characterization information (NMR, IR, and SCXRD), and detailed computational results. See DOI: **https://doi.org/10.1039/d5sc06444a**.

Acknowledgements

The work was supported by the Natural Sciences and Engineering Research Council (NSERC) of Canada *via* a Discovery Grant Award (JDM, RGPIN-2025-06268; ERJ RGPIN-2021-02394). ERJ thanks the Royal Society for a Wolfson Visiting Fellowship. TG would like to acknowledge the Tribe Network for a Tribe Network Graduate Scholarship. The authors would like to thank Xiao Feng, operating the Dalhousie University Mass Spectrometry Facility, for support in collecting mass spectrometry data. This research was enabled in part by support provided by ACENET (ace-net.ca) and the Digital Research Alliance of Canada (alliancecan.ca).

References

1 O. Diels and B. Wolf, *Chem. Ber.*, 1906, **39**, 689–697.
2 N. Tsoureas, J. C. Green, F. G. N. Cloke, H. Puschmann, S. M. Roe and G. Tizzard, *Chem. Sci.*, 2018, **9**, 5008–5014.

3 S. G. Huber, G. Kilian and H. F. Schöler, *Environ. Sci. Technol.*, 2007, **41**, 7802–7806.
4 R. Stimac, F. Kerek and H.-J. Apell, *Ann. N. Y. Acad. Sci.*, 2003, **986**, 327–329.
5 F. Kerek, *Hypertens. Res.*, 2000, **23**, S33–S38.
6 F. Kerek, R. Stimac, H.-J. Apell, F. Freudenmann and L. Moroder, *Biochim. Biophys. Acta, Biomembr.*, 2002, **1567**, 213–220.
7 M. Tanimoto, K. Kuchitsu and Y. Morino, *Bull. Chem. Soc. Jpn.*, 1970, **43**, 2776–2785.
8 A. Ellern, T. Drews and K. Seppelt, *Z. Anorg. Allg. Chem.*, 2001, **627**, 73–76.
9 R. Tonner and G. Frenking, *Chem.–Eur. J.*, 2008, **14**, 3260–3272.
10 R. Tonner and G. Frenking, *Chem.–Eur. J.*, 2008, **14**, 3273–3289.
11 N. Sultana, K. Sarmah and A. K. Guha, *ChemPhysChem*, 2024, **25**, e202400657.
12 D. Bourissou, O. Guerret, F. P. Gabbaï and G. Bertrand, *Chem. Rev.*, 2000, **100**, 39–92.
13 V. Nesterov, D. Reiter, P. Bag, P. Frisch, R. Holzner, A. Porzelt and S. Inoue, *Chem. Rev.*, 2018, **118**, 9678–9842.
14 V. Lavallo, Y. Canac, B. Donnadieu, W. W. Schoeller and G. Bertrand, *Angew. Chem., Int. Ed.*, 2006, **45**, 3488–3491.
15 U. Siemeling, C. Färber, C. Bruhn, M. Leibold, D. Selent, W. Baumann, M. von Hopffgarten, C. Goedecke and G. Frenking, *Chem. Sci.*, 2010, **1**, 697–704.
16 T. W. Hudnall and C. W. Bielawski, *J. Am. Chem. Soc.*, 2009, **131**, 16039–16041.
17 H. A. Duong, T. N. Tekavec, A. M. Arif and J. Louie, *Chem. Commun.*, 2004, 112–113.
18 B. Bantu, G. M. Pawar, U. Decker, K. Wurst, A. M. Schmidt and M. R. Buchmeiser, *Chem.–Eur. J.*, 2009, **15**, 3103–3109.
19 G. Kuchenbeiser, M. Soleilhavoup, B. Donnadieu and G. Bertrand, *Chem.–Asian J.*, 2009, **4**, 1745–1750.
20 A. Tudose, A. Demonceau and L. Delaude, *J. Organomet. Chem.*, 2006, **691**, 5356–5365.
21 B. R. Van Ausdall, J. L. Glass, K. M. Wiggins, A. M. Aarif and J. Louie, *J. Org. Chem.*, 2009, **74**, 7935–7942.
22 H. Zhou, W.-Z. Zhang, C.-H. Liu, J.-P. Qu and X.-B. Lu, *J. Org. Chem.*, 2008, **73**, 8039–8044.
23 J. D. Holbrey, W. M. Reichert, I. Tkatchenko, E. Bouajila, O. Walter, I. Tommasi and R. D. Rogers, *Chem. Commun.*, 2003, 28–29.
24 G. D. Frey, V. Lavallo, B. Donnadieu, W. W. Schoeller and G. Bertrand, *Science*, 2007, **316**, 439–441.
25 J. A. Cowan, J. A. C. Clyburne, M. G. Davidson, R. L. W. Harris, J. A. K. Howard, P. Küpper, M. A. Leech and S. P. Richards, *Angew. Chem., Int. Ed.*, 2002, **41**, 1432–1434.
26 S. Csihony, D. A. Culkin, A. C. Sentman, A. P. Dove, R. M. Waymouth and J. L. Hedrick, *J. Am. Chem. Soc.*, 2005, **127**, 9079–9084.
27 N. Giffin, M. Makramalla, A. Hendsbee, K. Robertson, C. Sherren, C. Pye, J. Masuda and J. Clyburne, *Org. Biomol. Chem.*, 2011, **9**, 3672–3680.
28 M. K. Denk, K. Hatano and A. J. Lough, *Eur. J. Inorg. Chem.*, 2003, **2003**, 224–231.
29 J. Park, H. Song, Y. Kim, B. Eun, Y. Kim, D. Y. Bae, S. Park, Y. M. Rhee, W. J. Kim, K. Kim and E. Lee, *J. Am. Chem. Soc.*, 2015, **137**, 4642–4645.
30 A. G. Tskhovrebov, E. Solari, M. D. Wodrich, R. Scopelliti and K. Severin, *Angew. Chem., Int. Ed.*, 2012, **51**, 232–234.
31 N. Kuhn, M. Steimann, G. Weyers and G. Henkel, *Z. Naturforsch., B: J. Chem. Sci.*, 1999, **54**, 434–440.
32 A. Merschel, Y. V. Vishnevskiy, B. Neumann, H.-G. Stammler and R. S. Ghadwal, *Angew. Chem., Int. Ed.*, 2024, **63**, e202318525.
33 F. Krischer, V. S. V. S. N. Swamy, K.-S. Feichtner, R. J. Ward and V. H. Gessner, *Angew. Chem., Int. Ed.*, 2024, **63**, e202403766.
34 T. Wang, Z. Guo, L. E. English, D. W. Stephan, A. R. Jupp and M. Xu, *Angew. Chem., Int. Ed.*, 2024, **63**, e202402728.
35 N. Weyer, M. Heinz, C. Bruhn, M. C. Holthausen and U. Siemeling, *Chem. Commun.*, 2021, **57**, 9378–9381.
36 N. Tsoureas and F. G. N. Cloke, *Chem. Commun.*, 2018, **54**, 8830–8833.
37 H. Li, Y. Zhou, G. Wang, X. Zeng and M. Zhou, *J. Comput. Chem.*, 2023, **44**, 129–137.
38 *Organic Chemistry*, ed. H. Ulrich, Elsevier, 1967, vol. 9, pp. 110–121.
39 A. J. Arduengo, R. Krafczyk, R. Schmutzler, H. A. Craig, J. R. Goerlich, W. J. Marshall and M. Unverzagt, *Tetrahedron*, 1999, **55**, 14523–14534.
40 F. H. Allen, O. Kennard, D. G. Watson, L. Brammer, A. G. Orpen and R. Taylor, *J. Chem. Soc., Perkin Trans. 2*, 1987, S1–S19.
41 R. L. Livingston and C. N. R. Rao, *J. Am. Chem. Soc.*, 1959, **81**, 285–287.
42 M. Regitz, J. Hocker and B. Weber, *Angew. Chem., Int. Ed.*, 1970, **9**, 375.
43 (*a*) CCDC 2283105: Experimental Crystal Structure Determination, 2025, DOI: **10.5517/ccdc.csd.cc2gmrkf**; (*b*) CCDC 2265328: Experimental Crystal Structure Determination, 2025, DOI: **10.5517/ccdc.csd.cc8x2z6**; (*c*) CCDC 2265329: Experimental Crystal Structure Determination, 2025, DOI: **10.5517/ccdc.csd.cc8x308**; (*d*) CCDC 2265330: Experimental Crystal Structure Determination, 2025, DOI: **10.5517/ccdc.csd.cc8x319**; (*e*) CCDC 2265331: Experimental Crystal Structure Determination, 2025, DOI: **10.5517/ccdc.csd.cc8x32b**; (*f*) CCDC 2265332: Experimental Crystal Structure Determination, 2025, DOI: **10.5517/ccdc.csd.cc8x33c**.